ACCSCIENCE PUBLISHING

Materials Science in Additive Manufacturing

REVIEW ARTICLE

Ceramic additive manufacturing via vat photopolymerization

Chongyu Long[1], Zhiyuan Liu[1,2], Changyong Liu[1,2], and Zhangwei Chen[1,2]*

[1]Additive Manufacturing Institute, Shenzhen University, Shenzhen, Guangdong, China

[2]Guangdong Key Laboratory of Electromagnetic Control and Intelligent Robotics, Shenzhen University, Shenzhen, Guangdong, China

(This article belongs to the *Special Issue*: *Additive Manufacturing of High Performance Ceramics*)

Abstract

Vat photopolymerization (VPP) additive manufacturing has emerged as a transformative approach for fabricating high-performance ceramic components with intricate geometries. This review comprehensively examines VPP technologies, including stereolithography, digital light processing, and two-photon polymerization, highlighting their mechanisms, advantages, and limitations. Critical challenges faced by ceramic VPP include light scattering from particles, slurry viscosity control, sedimentation, and post-processing shrinkage. The required optimized characteristics suitable for VPP of ceramic slurries and pre-ceramic polymers are also discussed. The latter offers a promising alternative, enabling the shaping of complex architectures with reduced defects and enhanced thermal stability, supported by active/passive fillers that mitigate shrinkage and improve density. Ceramic VPP applications span biomedical implants, microreactors, aerospace components, and energy devices. Key advancements include the integration of multimaterial systems, hybrid precursors, and nanocomposites. However, challenges persist in achieving uniform curing depths, minimizing anisotropic shrinkage, and scaling production. Future research should focus on material innovation, process parameter optimization, and advanced characterization techniques to unlock the full potential of VPP for next-generation ceramic manufacturing. This technology offers an effective solution for high-value ceramic applications.

Keywords: Ceramics; Vat photopolymerization; Stereolithography; Slurries; Sintering

***Corresponding author:**
Zhangwei Chen
(chen@szu.edu.cn)

Citation: Long C, Liu Z, Liu C, Chen Z. Ceramic additive manufacturing via vat photopolymerization. *Mater Sci Add Manuf.* 2025;4(3):025200031. doi: 10.36922/MSAM025200031

Received: May 13, 2025

Revised: June 3, 2025

Accepted: June 4, 2025

Published online: July 11, 2025

1. Introduction

Additive manufacturing technologies have revolutionized the way we produce complex parts, offering a layer-by-layer approach to creating both two-dimensional (2D) and three-dimensional (3D) components directly from computer-aided design (CAD) models.[1] These advanced techniques have attracted great attention for their capability of producing intricate geometries without the need for additional tooling, making them highly cost-effective for rapid prototyping and final part production. The additive manufacturing landscape is diverse, encompassing seven main categories, including powder bed fusion, binder jetting, material extrusion, and vat photopolymerization (VPP).[2] Among them, VPP technologies stand out for their scalability and ability to produce features ranging from micrometers to full-sized components.[3]

VPP is based on the principle of selectively curing a photosensitive liquid resin contained in a shallow vat through layer-by-layer photo-initiated crosslinking.[3] An automated ultraviolet (UV) light source, guided by a 3D CAD model, is directed across the resin surface to cure it in a precise, controlled manner. This process requires a support structure during the build phase, which is lowered after each layer is cured. The versatility and scalability of VPP techniques make them particularly suitable for creating complex features in various photosensitive polymers. While VPP is commonly associated with stereolithography (SL) for rapid prototyping, its application in ceramic fabrication has also garnered considerable attention.

Ceramics, known for their high hardness, wear resistance, corrosion resistance, and biocompatibility, have been extensively applied in industries such as mechanical engineering, electronics, and biomedical engineering.[4] Traditional ceramic manufacturing methods often involve complex and time-consuming steps, such as casting, injection molding, and pressing, which can limit the production of complex geometries. By offering a promising alternative, VPP enables the direct fabrication of ceramic parts with intricate designs and high precision.[2] This review paper focuses on the various VPP technologies used for ceramic fabrication, their advantages, and applications.

The preparation of ceramic objects using VPP technologies typically involves the use of ceramic slurries, which are composed of ceramic particles, resins, photoinitiators, dispersants, *etc.* These slurries should maintain suitably large solid content and reduced viscosity to ensure good printability and shape retention. The addition of dispersants helps achieve a homogeneous dispersion of ceramic powder in the slurry, which is beneficial to the printing process. However, incorporating ceramic particles into the slurry can pose several challenges, such as dispersion issues, viscosity problems, sedimentation, and stability concerns. These challenges need to be addressed to optimize the printing process and produce high-quality ceramic parts. In recent years, the development of pre-ceramic polymers has opened up new possibilities for ceramic fabrication using VPP technologies. These polymers can be easily shaped and formed and offer exceptional thermal stability, high strength, and fracture toughness compared to traditional ceramic powders. Using pre-ceramic polymers could prevent many of the issues associated with ceramic slurries, such as drying problems, long processing times, and the need for flammable solvents. This review also discusses the use of pre-ceramic polymers in VPP technologies, highlighting their advantages and potential applications in the fabrication of advanced ceramic components.

2. VPP techniques suitable for ceramic fabrication

2.1. Linear scanning SL

SL is regarded as the oldest rapid prototyping process and was invented by Hull in 1986.[5] The process requires the creation of a 3D CAD model and its conversion to an STL file, which is sent to the build station control software. The part is cut into a series of 2D slices of adequate thickness and the model becomes ready to print. A support platform is lowered into a vat of photocurable epoxy acrylate liquid resin so that it rests below a surface of approximately equal to the desired thickness. In linear scanning SL, a UV laser of nearly 100 milliwatts of power of fine beam diameter is directed onto the resin using a series of computer-controlled mirrors.[6] The laser causes the resin to polymerize and solidify it in a precise manner. Now, the platform is moved down with a single layer thickness to ensure that the new level is recoated to the layer of liquid resin. The laser then selectively solidifies the next layer and the overall process is repeated until the final object is built. Upon the completion of the model, the platform is raised up and out of the resin to allow the unsolicited resin to drain away. Further, after removing from the machine any excess resin and support structure are removed and the part is cleaned using suitable organic solvent to remove any uncured resin. The printed part is then cleaned using air and water to remove the solvent and is then placed in a UV oven in order to cure and fully solidify it. Finally, the model can be sanded down using ultra-fine sandpaper to obtain a smooth surface finish. The SL technique is commonly used for creating small-to-medium-sized concept models or prototypes for aerodynamic testing in wind tunnels as well as parts with fine details such as those used in the preparation of scaffolds for tissue engineering, optical, and microelectromechanical system (MEMS)/nanoelectromechanical system devices.

Materials used in SL are normally liquid resins with an appropriate proportion of photoinitiators.[7] SL is not preferred to create chemically functionalized parts due to the fixed composition of the resins and may require post-printing functionalization, if possible in some cases.[8] It is also possible to interchange containers filled with different materials for multimaterial printing of single objects through the SL process.[9] For printing of ceramic parts using SL, ceramic slurries with resins or pre-ceramic precursors are used to create green bodies, and further their processing at high temperatures are performed to obtain high-quality ceramic parts.[10] Light scattering is a challenging factor influencing the printing quality for ceramic powder slurries, while the pre-ceramic precursors are best suited for printing purposes. SL-printed parts are of high resolution due to a laser of fine diameter, which is scanned with high accuracy. The

limitation with SL is the requirement of the build platform, which has to be mechanically removed, necessitating surface finishing. Figure 1A shows the SL working principle. The fundamental mechanism of photopolymerization is that the resin surface is exposed to UV light to trigger polymerization via single-photon absorption by the photoinitiator.

The mechanism of the linear photo-polymerization process involved in linear laser SL is shown in Figure 2B. A single-photon is absorbed by the photoinitiator (Figure 2A) to form free radicals triggering the cross-linking of the monomers. Because of the Gaussian nature of the incident light beam, the number of photons hitting the resin surface will be maximum at the center of the laser spot and will decay away from it. This leads to the parabolic cross-section in the resin during each laser scan. The depth of the parabola, *i.e.*, cure depth (C_d) of the resin is related to the exposure energy and is given by Beer–Lambert law as:

$$C_d = S_d \ln\left(\frac{E}{E_c}\right) \quad \text{(I)}$$

where E is the exposure energy, E_c is the critical exposure energy and S_d is the transmission depth coefficient of the resin. S_d and E_c remain constant for a fixed recipe of resin/slurry.

This cure depth is measured and calibrated to derive a log-linear relationship between the cure depth of the resin and the exposure power. The laser spot size determines the feature size. Further, there must be good adhesion between the lateral lines and the vertical layers of the model to obtain a contiguous full-density part.

In SL, where foreign materials such as ceramic particles are incorporated inside the resin, the polymerization process is influenced significantly by the particle size, and the relationship between the cure depth and the particle size is described as:[11]

$$C_d = \frac{d}{Q}\frac{1}{\varphi}\ln\left(\frac{I_0}{I_{cure}}\right) \quad \text{(II)}$$

where φ = ceramic solid loading, d = ceramic powder size, Q = suspension constant, I_0 = exposure intensity, and I_{cure} = the critical exposure intensity for the suspension. Thus, greater ceramic particles result in larger cure depth as the scattering effect is reduced.[2] Smaller-diameter ceramic particles, which show strong scattering, would lead to lower cure depth. However, small particles are desired for increasing the solid loading printing and lowering the sintering temperature, which is good for the final ceramic products. In terms of the effect of particle shape, the semi-liquid nature of the ceramic slurry is generally favorable in favor of flowability, and there is no specific requirement for particle sphericity and regularity.

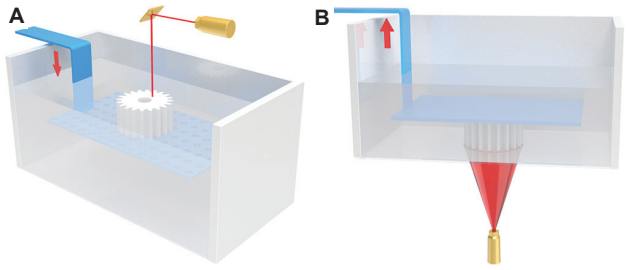

Figure 1. Schematic setup of linear scanning stereolithography technique (A) and image projection digital light processing (DLP) technique (B)[2] (schematics reused under the terms of the Creative Commons CC-BY license)

2.2. Planar photopolymerization based on DLP

DLP photopolymerization technique is based on a similar principle as laser SL, but it uses a conventional UV light source rather than a laser, and the patterns are transferred

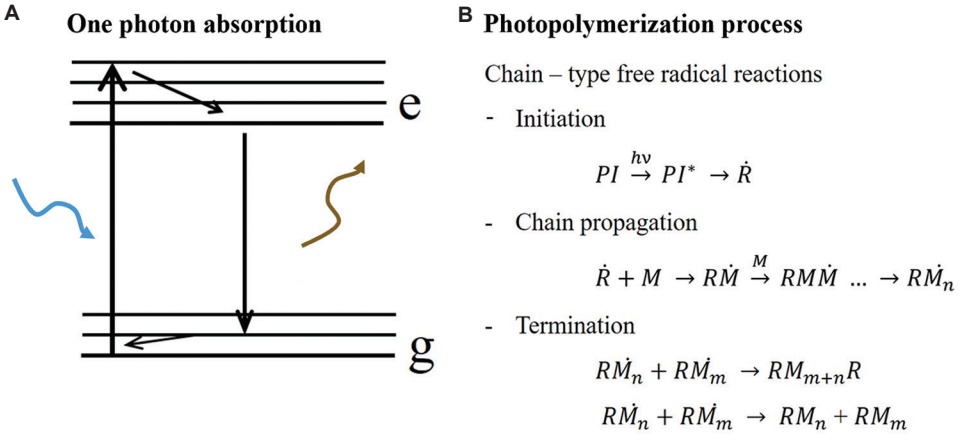

Figure 2. Single-photon absorption mechanism (A) and polymerization mechanism in linear stereolithography and digital light processing (B)

to resin by projecting an entire slice of the 2D model (Figure 1B). For the projection of the slice pattern onto the resin, a digital micromirror device (DMD) panel is used, making the DLP printing process faster than SL and facilitating quick fabrication of highly accurate parts with excellent resolution, resembling the products made with SL. DLP also requires a support platform, and structures need to be removed manually and may require finishing. The concept of DLP was first developed in 1996.[12] Further in 1997, liquid crystal display was replaced by DMDs to create high resolution and contrast in the projected pattern.[13] DMD is an array of microscopic mirrors that are capable of swift rotation within a range of ±10–12°.

2.3. Two-photon polymerization (TPP)

TPP, as illustrated in Figure 3, utilizes the two-photon absorption mechanism, in which molecules transition from ground to excited states through simultaneous absorption of two laser photons – either with identical energy (termed degenerate two-photon absorption [TPA]) or distinct energy levels (non-degenerate TPA). This mechanism demands intense photon flux due to the molecule's extremely brief residence (10^{-18} s) in the transient virtual state, necessitating ultrashort-pulsed infrared lasers to achieve sufficient energy delivery. TPA was theoretically predicted by Göppert-Mayer[14] in 1931 and the experimental observation was confirmed by Kaiser and Garrett[15] in 1961. Nowadays, the TPA process has become extensively important for technological applications, such as multiphoton polymerization, multiphoton optical limiters, and multiphoton fluorescence spectroscopy.

In conventional single-photon absorption (*e.g.*, in SL or DLP printing), excitation occurs when incident photon energy matches the electronic transition energy between ground and excited states, resulting in a linear photon flux dependence. Conversely, TPA requires simultaneous absorption of two lower-energy photons. During TPA, the molecule enters a short-lived virtual intermediate state after the first photon absorption. This mechanism enables UV-sensitive photoinitiators (350 – 400 nm) to be activated by near-infrared Ti: Sapphire lasers (700 – 800 nm) through TPA.

As a third-order nonlinear optical phenomenon,[17] degenerate TPA exhibits an energy absorption rate expressed as:

$$\frac{dW}{dt} = \frac{8\pi^2\omega}{c^2n^2} I^2 \,\mathrm{Im}[\chi^{(3)}] \tag{III}$$

where ω represents the angular frequency, c denotes the speed of light in a vacuum, and n is the refractive index of the medium. The nonlinear optical response arises from the imaginary component of the third-order susceptibility ($\mathrm{Im}[\chi^{(3)}]$), with the TPA process exhibiting a quadratic dependence on laser intensity. Due to this nonlinear intensity dependence, TPA occurs only at extremely high optical intensities, necessitating high-numerical-aperture (NA) microscope objectives for tight laser focusing. The TPA effect rapidly diminishes away from the focal center, resulting in a well-defined 3D voxel that enables intrinsic volumetric fabrication in two-photon lithography. The polymerization threshold is determined by the balance between radical generation (initiated by TPA) and competing deactivation pathways, including quenching, internal conversion, and radical termination.[18] Below this threshold, insufficient crosslinking occurs, while above

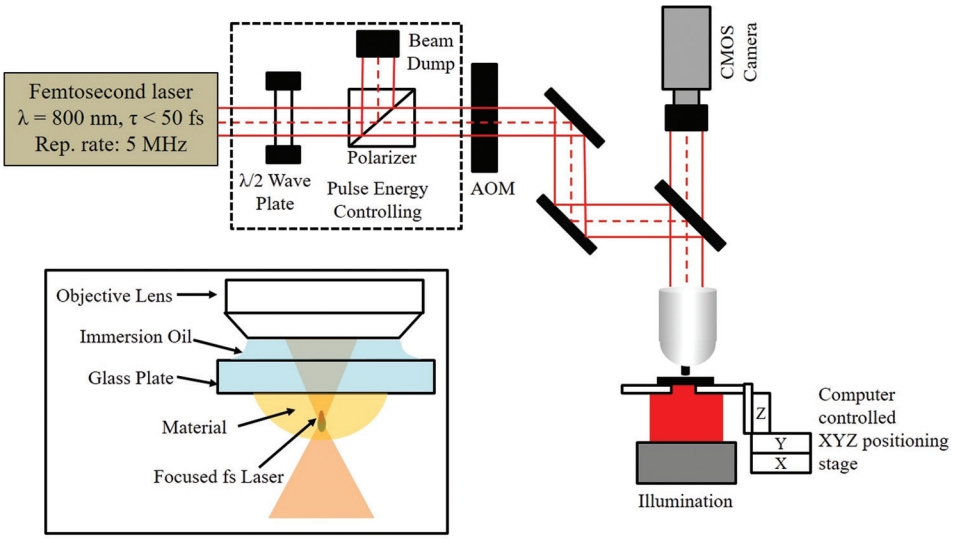

Figure 3. Schematic diagram of two-photon polymerization process[16] (schematic reused under the terms of the Creative Commons CC-BY license)

it, stable solid structures form. The threshold is further influenced by the TPA cross-section (δ) of the photoinitiator, which quantifies the probability of simultaneous photon absorption per unit time (Equation IV):

$$\frac{dn_p}{dt} = \delta N F^2 \quad \text{(IV)}$$

where N denotes the molecular number density (absorbing molecules per unit volume), while $F = I/h\nu$ represents the incident photon flux, where h is Planck's constant and ν is the optical frequency. Since:

$$\frac{dW}{dt} = \frac{dn_p}{dt} h\nu \quad \text{(V)}$$

Hence, δ can be expressed as:

$$\delta = \frac{16\pi^3 h\nu^2}{c^2 n^2 N} \mathrm{Im}[\chi^{(3)}] \quad \text{(VI)}$$

where δ has a unit of 10^{-58} m^4s/photon.[14]

Upon TPA, a portion of the excited initiator undergoes intersystem crossing to the triplet state, followed by bond cleavage to generate reactive radicals or ionic species, thereby initiating TPP. The efficiency of radical formation, termed radical quantum yield (φ), combined with the TPA cross-section (δ), determines the initiator's performance. Optimizing these parameters enables efficient TPP at reduced laser power and higher writing speeds.[17] The lifetime of radicals and polymerization kinetics are influenced by multiple factors, such as radical quenching (*e.g.*, by oxygen or other radicals), intramolecular recombination, and chain transfer reactions with surrounding molecules. These dynamics vary depending on the photoinitiator, monomer, solvent, and environmental conditions (*e.g.*, temperature, atmosphere), ultimately affecting achievable resolution and processing parameters.[19] Although the theoretical resolution limit of TPP is extremely small – determined by the voxel dimensions at the polymerization threshold – practical feature sizes are constrained by laser stability, material composition, and the numerical aperture (NA) of the focusing objective.[20] For high-NA objectives (NA > 0.7), the optical resolution can be estimated using the following equations:[21]

$$r_{xy} = \frac{0.325\lambda}{\sqrt{2} NA^{0.91}} \quad \text{(VII)}$$

$$r_z = \frac{0.532\lambda}{\sqrt{2}} \left[\frac{1}{n - \sqrt{n^2 - NA^2}} \right] \quad \text{(VIII)}$$

where r_{xy} and r_z denote the lateral and axial resolution limits, respectively; λ represents the excitation wavelength; n is the medium's refractive index; and NA corresponds to the objective's NA.

2.4. Continuous liquid interface production

Traditional SL methods employ a layer-by-layer approach, resulting in slow printing speeds unsuitable for mass production. In addition, oxygen inhibition during photopolymerization often leads to incomplete curing by either deactivating photoinitiators or forming peroxides.[22] To address these limitations, Tumbleston *et al.* introduced continuous liquid interface production (CLIP), an advanced SL technique.[22] In CLIP, printing occurs above an oxygen-permeable window, forming a thin "dead zone" (tens of micrometers thick) where oxygen suppresses curing. This uncured layer prevents adhesion between the window and the printed part, enabling continuous fabrication. As illustrated in Figure 4, CLIP operates by projecting UV images through a transparent, oxygen-permeable window into a liquid resin. Unlike conventional SL, which requires intermittent resin renewal and layer repositioning, CLIP continuously draws the cured part upward while fresh resin flows into the dead zone. This eliminates stepwise interruptions, significantly boosting printing speeds – up to 500 mm/h or higher – without compromising resolution. Moreover, print speed remains independent of layer thickness, further enhancing efficiency. Key advantages of CLIP include: (i) elimination of oxygen inhibition via controlled dead zone formation; (ii) continuous printing without pauses for resin replenishment; (iii) high-speed production while maintaining precision; and (iv) flexibility in layer thickness without affecting speed. This innovation overcomes critical drawbacks of conventional SL, making it viable for scalable, high-throughput manufacturing.

The CLIP process critically depends on establishing an oxygen-inhibited dead zone, achieved through an amorphous fluoropolymer window that combines high oxygen permeability with UV transparency and chemical resistance. The dead zone's thickness is determined through differential measurement techniques and varies with both oxygen availability and the window's permeability characteristics. Key observations include: (i) When using ambient air instead of pure oxygen, the dead zone thickness approximately doubles. (ii) Increasing photon flux reduces the dead zone thickness. (iii) Nitrogen environments completely eliminate the dead zone, preventing CLIP operation. For systems operating with ambient air, the dead zone thickness can be calculated as:

$$Dead\ zone\ thickness = C\left(\frac{\varphi_0 \alpha_{PI}}{D_{c0}}\right)^{-0.5} \quad \text{(ix)}$$

where φ_0 is the intensity of incident photons, α_{PI} is the product of photoinitiator concentration and the wavelength-dependent absorptivity, D_{c0} is the resin reactivity, and C is a

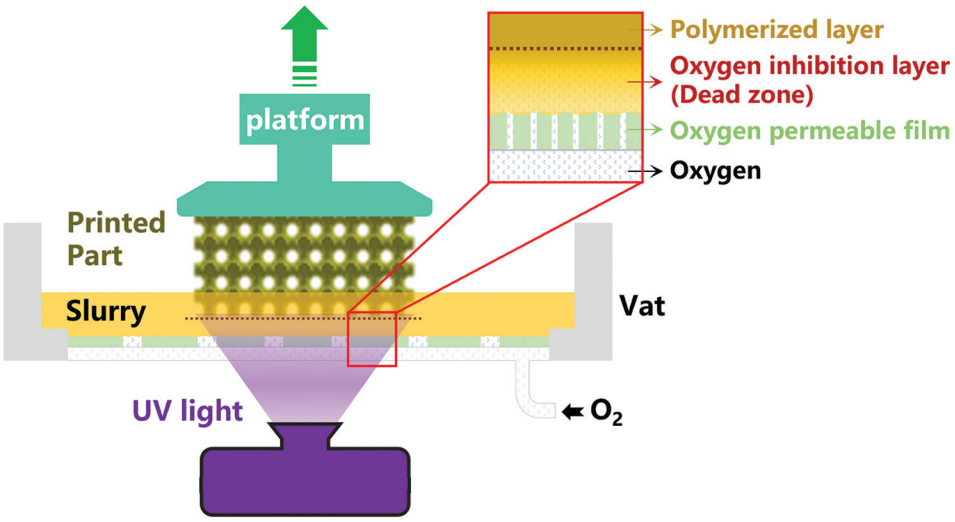

Figure 4. The working principle of continuous liquid interface production technology enables rapid, continuous fabrication without traditional layer-by-layer deposition. The system operates by simultaneously raising the build platform while dynamically updating projected ultraviolet cross-sectional patterns through an oxygen-permeable window. A critical feature is the maintenance of a thin uncured region (dead zone) at the interface between the growing part and the permeable window, allowing for uninterrupted printing.

proportionality constant. An increase in either φ_0 or α_{PI} leads to an increase in free radicals and a decrease in the initial oxygen. The oxygen permeating through the window gradually decreases in concentration as it penetrates deeper into the resin. This creates a concentration gradient where free radicals eventually dominate over oxygen inhibition at a specific penetration depth. The critical polymerization threshold is reached when oxygen depletion occurs while sufficient free radicals remain active. Enhancing the photoinitiation efficiency reduces this threshold distance, consequently decreasing the thickness of the oxygen-rich inhibition layer. The constant C in this system correlates with the square root of the membrane's oxygen diffusion coefficient. Furthermore, maintaining a consistent dead zone requires precise control of oxygen flux, which is determined by the membrane's permeability-to-thickness ratio.[23] The resulting cured layer thickness can be expressed by the following relationship:

$$Cured\ thickness = C\left(\frac{\varphi_0 \alpha_{PI}}{D_{c0}}\right)^{-0.5} \quad \text{(X)}$$

where t is the exposure time and α is the absorption coefficient of the resin. The relation between the print speed, resolution (h_A), and dead zone thickness is given by the following relation:

$$\frac{\text{Speed}}{h_A} = \left(\frac{\varphi_0 \alpha_{PI}}{D_{c0}}\right), \text{where} h_A = 1/\alpha \quad \text{(XI)}$$

The printing speed can be enhanced by optimizing process parameters for a given layer thickness (h_A). However, excessive speed reduction in dead zone thickness may compromise process stability, with critical thresholds typically ranging from 20 μm to 30 μm to avoid adhesion-related defects. When operating at minimal zone thickness, resolution compromises become necessary for further speed improvements. For large solid cross-sections, resin characteristics such as viscosity and pressure gradients require careful optimization. CLIP technology demonstrates versatility across material classes including elastomers, ceramics, and biomaterials, offering advantages in the rapid, cost-effective production of complex geometries. Ongoing research continues to expand its applications, particularly in pre-ceramic material systems. Table 1 summarizes the key characteristics of VPP methods.

3. Materials and process parameters

The VPP technique requires careful formulation of ceramic suspensions to achieve optimal printing performance, mechanical strength, and post-treatment characteristics. The manufacturing sequence involves four key stages: forming, polymerization, thermal decomposition, and ceramic conversion. These ceramic suspensions typically consist of five main components: ceramic particulates, photocurable polymers, light-sensitive initiators, stabilizing agents, and supplementary modifiers. Critical formulation requirements include high ceramic loading with maintained fluidity for successful printing and dimensional stability and effective particle dispersion through stabilization additives to ensure homogeneous microstructures.

Table 1. Comparative analysis of vat photopolymerization methods suitable for ceramic component production

Technology	Features	Power Source	Material type	Shaping method	Requirements	Accuracy
SL	Limited speed, intermediate cost, good efficiency, high surface quality	UV Laser	Slurry	Linear polymerization	UV-polymerizable and solvent-cleavable molecular units	<100 μm
DLP	Fast speed, intermediate cost, good efficiency, high surface quality	UV Source	Slurry	Linear polymerization	UV-polymerizable and solvent-cleavable molecular units	<100 μm
TPP	Limited speed, expensive, superior surface quality, optimal printing precision	IR Laser	Slurry	Nonlinear polymerization	IR-polymerizable and TPA molecular units	<1 μm
CLIP	Faster speed, intermediate cost, high efficiency, high surface quality	UV Source	Slurry	Linear Polymerization	UV-polymerizable and solvent-cleavable molecular units	<100 μm

Abbreviations: CLIP: continuous liquid interface production; DLP: digital light processing; IR: infrared; SL: stereolithography; TPA: two-photon absorption; TPP: two-photon polymerization; UV: ultraviolet.

Common ceramic powders used include oxide ceramics (*e.g.*, alumina [Al_2O_3] and zirconia [ZrO_2]), and non-oxide ceramics (*e.g.*, SiC, Si_3N_4, and AlN). Advanced composites, such as cordierite and Li_4SiO_4 systems, are also employed to enhance mechanical and thermal properties. The addition of ceramic powder into the photopolymers can cause several problems:

(i) *Dispersion issues.* Ceramic particles tend to aggregate due to interparticle forces such as van der Waals forces and electrostatic interactions. This aggregation can lead to an uneven distribution of particles in the slurry, resulting in defects in the printed parts. For example, in the preparation of alumina slurries, if the dispersion is not good, it may cause the formation of pores and cracks in the sintered parts

(ii) *Viscosity problems.* As the amount of ceramic powder increases, the viscosity of the slurry generally increases. High viscosity can affect the flowability of the slurry, making it difficult to fill small features and complex structures during printing

(iii) *Sedimentation and stability.* Ceramic particles are denser than the liquid medium, and they may settle under gravity over time, causing the slurry to become unstable. This sedimentation can lead to a non-uniform distribution of particles in the printed parts, affecting their properties. According to Stokes' sedimentation law, reducing the particle size, increasing the fluid viscosity, and increasing the solid fraction can help stabilize the slurry

(iv) *Shrinkage and deformation.* During the sintering process, the ceramic parts may experience shrinkage and deformation. The lower the solid content in the slurry, the greater the shrinkage rate of the green part. This can influence the structural accuracy and integrity of the final parts

(v) *Binder removal difficulties.* The binder added to the slurry needs to be removed before sintering. If the binder content is high, the debinding process becomes more difficult. The formation of a large amount of gas in the binder removal step can cause stresses, part cracking, and deformation.

More importantly, the addition of ceramic particles would cause absorption and scattering of incident light, which can significantly affect the printing quality in VPP 3D printing.

(i) *Curing depth reduction.* Ceramic particles absorb and scatter light, reducing the intensity of light that reaches deeper layers of the slurry. This leads to a decrease in curing depth. As the solid loading of ceramic particles increased, the light transmittance of the suspension significantly decreased, resulting in a reduction in curing depth. The reduction in curing depth and the increase in curing width can lead to a decrease in the curing ability

(ii) *Curing width increase.* The scattering of light causes the light to spread out, leading to an increase in curing width. This can result in the blurring of the edges of the printed features, reducing the printing resolution and accuracy. The scattering of light in the lateral direction can cause the printed features to be larger than the designed size. This is because the scattered light can cure the resin in the surrounding areas, leading to an increase in the size of the printed features. The scattering of light can also affect the fidelity of the printed features. For example, the edges of the printed features may be blurred or rounded, and the details of the features may be lost, leading to reduced overall quality of the printed parts.

To compensate for the effects of light absorption and scattering, it may be necessary to optimize the printing parameters, such as the light intensity, exposure time, and layer thickness. This can be a complex and time-consuming process and may require extensive experimentation and testing.

For a ceramic slurry to be compatible and printable with VPP, it should have some common features and requirements:

(i) *Composition.* Ceramic slurries consist of ceramic powders (40 – 60 vol.%), UV-curable resins (*e.g.*, acrylates), photoinitiators, and dispersants. For instance, alumina-based slurries with optimized particle size distributions (coarse, medium, and fine powders) improve packing density and reduce defects

(ii) *Rheology.* Low viscosity (<3 Pa·s) is critical for layer uniformity, achieved by balancing solid loading and dispersant content. High solid loading (>50 vol.%) ensures structural stability but risks increased viscosity. Sedimentation and agglomeration of particles can compromise print quality, necessitating continuous agitation

(iii) *Photoreactivity.* Slurries must allow sufficient UV penetration for curing. Nanoparticle additives (*e.g.*, SiC and YAG) can enhance properties but may scatter light, requiring precise formulation.

In recent years, the persistent challenges in formulating ceramic slurries and optimizing VPP processes have prompted the exploration of alternative ceramic feedstock materials. Among these, pre-ceramic polymer-derived ceramics have gained significant research interest due to their superior processability during shaping operations and outstanding material properties. Compared to conventional powder-based ceramic processing, these polymer-derived materials demonstrate remarkable thermal stability along with enhanced mechanical characteristics, including higher strength and improved fracture toughness.

Pre-ceramic polymers can be directly processed through sol-gel methods, offering advantages such as simplified handling, no drying issues, shorter processing times, elimination of flammable solvents, and superior solution stability compared to ceramic powders or pastes. A critical aspect of pre-ceramic polymer processing is crosslinking, which is essential for ceramic formation. Adjusting the molecular weight of these polymers enables precise control over rheological properties, an area of ongoing research.[24] The rheological behavior of pre-ceramic polymers is particularly crucial when they serve as binders for ceramic powders in composite printing applications. Silicon-based pre-ceramic polymers are widely utilized in SL for fabricating intricate structures due to their stability. These photocurable inorganic polymers transform into high-strength, chemically inert ceramics upon pyrolysis in inert atmospheres. The incorporation of active or passive fillers allows for the creation of diverse advanced ceramic phases.[2,25] An optimal pre-ceramic polymer should exhibit high molecular weight, suitable rheological properties, good solubility for shaping, and functional groups that facilitate curing and crosslinking.[26] Table 2 presents a summary of the commonly used organosilicon pre-ceramic polymers, along with their backbone structures, synthesis methods, and resulting ceramics.

In the VPP process, photopolymerizable monomers along with a small amount of photoinitiator and other additives are used to make a slurry/blend of appropriate rheological properties. Ceramic particles of sizes down to micro/nanometers can also be incorporated into it for the fabrication of composite ceramics[44] before printing. The processing and printing steps of pre-ceramic polymers

Table 2. List of commonly used pre-ceramic polymers for vat photopolymerization and ceramization along with their synthesis methods and respective derived ceramics

Pre-ceramic polymer	Derived ceramics	Applications	Ref.
Polysilanes ($-R_1R_2Si-$)	SiC	Photoresists, semiconductors, precursors to polycarbosilane synthesis	26-28
Polycarbosilane ($-R_1R_2Si-C-$)	SiC	Electric or photo-conductors, photoresists, nonlinear optical materials	29-33
Polysilazane ($-R_1R_2Si-N=$)	Si_3N_4 and SiCN	Barrier for heat exchanger, oxidation-resistant	34-36
Polysiloxane ($-R_1R_2Si-O-$)	SiOC	Biomedical, electronics, textile chemistry	37,38
Poly (organosilylcarbodiimides) ($-R_1R_2Si-N=C=N-$)	SiCN	High-temperature ceramics, chemically resistant	39,40
Polyborosilazane ($-R_1R_2Si-N(R_3R_4B)-$) Polyborosilane, ($-R_1R_2Si-B(R_3)-$) Polyborosiloxane ($-R_1R_2Si-O(R_3R_4B)-$)	Borosilicate ceramics such as SiCBN, SiBC, etc.	High-temperature ceramics, chemically resistant	41-43

starting from the primary precursors are shown in Figure 5. The final yield, y_c, of the ceramic is given as:

$$y_c = \frac{w_1}{w_0} \quad \text{(XII)}$$

where y_c is the ceramic yield, w_1 is the weight of ceramic residue, and w_0 is the original weight of the specimen before pyrolysis.

The cross-linking of pre-ceramic polymers is a critical step, typically achieved through radiation or catalytic methods at low temperatures. Polymers with a high degree of crosslinking exhibit improved ceramic yield, which is essential for maintaining structural integrity during subsequent processing. Most pre-ceramic polymers feature an inorganic backbone with hydrogen atoms or organic substituents. These components either integrate into the ceramic residue or are released as volatile byproducts during high-temperature pyrolysis. This conversion process involves gas evolution, isotropic shrinkage, and pore formation, often leading to structural defects that compromise the final ceramic density. To mitigate these issues, incorporating fillers has become a primary approach for producing bulk ceramic components with controlled dimensions. A variety of fillers – including polymeric, metallic, and ceramic materials in nano- or micro-scale forms – can be blended into pre-ceramic polymers to enhance their properties. Fillers play multiple functional roles and can be categorized as either reactive or passive. Passive fillers remain chemically stable throughout the entire process, showing no reactivity with the pre-ceramic polymer, ceramic residue, or processing atmosphere. Their primary function involves facilitating gas release during pyrolysis, which helps minimize dimensional shrinkage while preventing crack formation and macroporosity in the final ceramic product.[45] In contrast, active fillers chemically interact with both the gaseous byproducts of ceramization and the processing atmosphere, potentially altering the composition of the resultant ceramic material. These reactive additives enable precise tuning of functional characteristics, including electrical conductivity, thermal expansion behavior, and magnetic properties. Notably, when pre-ceramic polymers contain substantial filler content, the reinforcing effect of these additives may eliminate the need for crosslinking by providing sufficient structural support to maintain dimensional stability during processing.

4. Post-processing and heat treatment

Post-curing represents a critical secondary processing step that enhances the consolidation of incompletely polymerized resin components within fabricated structures. This treatment significantly improves the mechanical performance and structural integrity of printed components. However, substantial dimensional changes occurring during post-processing remain a key challenge in ceramic photopolymerization techniques. Consequently, comprehensive characterization of post-curing behavior is fundamental for minimizing geometric distortion and improving dimensional accuracy in printed ceramic components.

The curing shrinkage is primarily influenced by the curing extent of the green-state material[46] where higher curing degrees result in reduced shrinkage. The curing degree depends on process parameters such as laser power, layer pitch, scan pitch, and scanning speed. Increased laser power enhances crosslinking, improving curing depth and line width. Conversely, larger layers and scan pitches reduce curing by leaving more uncured resin, while faster scanning speeds decrease energy exposure per unit area. Laser power stability and resin photosensitivity (wavelength compatibility) further affect curing efficiency. Among these factors, laser power, layer pitch, and scan pitch play dominant roles in determining the final curing degree.

The curing efficiency demonstrates an inverse correlation with layer thickness, where the reduced spacing between layers promotes greater overlap and minimizes residual uncured resin. This relationship similarly governs scan spacing effects, as wider intervals leave more materials uncured and consequently diminish curing quality. Scanning velocity plays a crucial role, with faster speeds reducing energy deposition per unit area and thus lowering curing effectiveness. Process stability emerges as another critical factor, where fluctuations in laser power lead to inconsistent polymerization. The material's inherent properties, particularly its photosensitivity and spectral

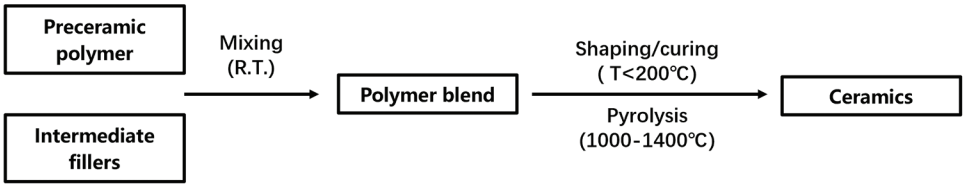

Figure 5. Processing steps involved to obtain ceramics from pre-ceramics
Abbreviations: R.T.: room temperature; T: temperature

compatibility with the irradiation wavelength, significantly influence photon absorption efficiency and curing outcomes. Among these interdependent parameters, laser power output, layer thickness setting, and scan spacing configuration exert the most substantial influence on the final curing performance.

The transformation of cured structures into ceramic components requires controlled thermal treatment, where sintering parameters critically influence the final material characteristics. Key processing variables including heating rate, atmospheric conditions, target temperature, and holding duration collectively govern phase formation and microstructural evolution by modulating crystallization behavior, carbothermal reactions, and filler interactions. During sintering, organic functional groups (methyl, phenyl, vinyl) are progressively removed from the polymer network, enhancing mechanical stability. Sintering defects evolve as the polymer binder burns out, creating initial voids, while simultaneous powder densification drives overall shrinkage. These small voids can coalesce into larger pores driven by capillary forces during particle rearrangement. Differential densification occurs when regions with varying green density (like thick vs. thin sections or near supports) shrink at different rates, generating stress, warping, or cracks propagating from denser areas or large pores. Control strategies include optimizing the polymer resin to pyrolyze cleanly, ensuring high and uniform powder packing in the green part, carefully controlled sintering profiles (temperature, time, atmosphere) for uniform densification, and software-based design compensation for isotropic shrinkage. For example, to minimize crack formation caused by gaseous byproduct evolution, heating rates must be carefully controlled, typically below 2°C/min, particularly within the critical polymer-to-ceramic transition range. Despite such precautions, ceramic products often exhibit residual porosity and microcracks due to inherent shrinkage. These limitations can be effectively mitigated through strategic filler incorporation, where reactive additives interact with either the pre-ceramic matrix or processing atmosphere to produce dense, crack-resistant ceramic composites.[27]

On the other hand, the sustainability of VPP demands attention. Key concerns include the recyclability of uncured resin slurry to minimize hazardous waste, the environmental impact of potentially toxic photoinitiators (driving research into safer alternatives), and the significant energy consumption during high-temperature sintering, a major carbon footprint contributor. Future strategies may focus on closed-loop slurry recycling systems, developing readily biodegradable resin systems and photoinitiators, optimizing sintering profiles, or adopting advanced sintering techniques to drastically reduce energy requirements over the part lifecycle.

5. Performance and applications

VPP enables the fabrication of intricate ceramic components that surpass the geometric capabilities of components generated by traditional additive manufacturing methods. The unique advantages of pre-ceramic polymers – including their processability, formability, and tunable molecular structure – make them particularly suitable for this technique, facilitating the production of specialized ceramic parts. These components demonstrate significant potential across multiple engineering fields, from biomedical implants to electrochemical systems, MEMS, and optical applications. The performance characteristics of the final products are governed by two critical factors: the material composition and the resulting microstructure, both of which are controlled through careful selection of raw materials and optimization of sintering parameters. To meet practical application requirements, the printed ceramic components must satisfy three essential criteria: sufficient mechanical strength, high surface quality, and dimensional accuracy relative to their digital design specifications.[47] To quantitatively validate sintered 3D-printed ceramic part quality, key characterization tools include X-ray diffraction for phase identification and crystallinity assessment, nanoindentation to measure localized hardness and elastic modulus, and X-ray computed tomography for non-destructive 3D visualization and quantification of internal porosity, pore size distribution, and density gradients. These techniques objectively confirm mechanical properties, phase purity, microstructural homogeneity, and the absence of macro-defects such as large voids or cracks resulting from uncontrolled shrinkage or pore coalescence during sintering. Integrating this characterization provides crucial feedback for optimizing printing and sintering parameters to achieve targeted final properties.

The SL has become a widely adopted technique for manufacturing high-performance ceramic components. The preparation of ceramic suspensions represents a critical step in this process, as it directly impacts both printing quality and final part integrity. Optimal ceramic suspensions must exhibit three key characteristics: uniform particle distribution, suitable rheological behavior, and extended colloidal stability. A significant challenge in suspension preparation involves balancing competing requirements. While higher ceramic loading reduces sintering shrinkage and improves densification, excessive solid content increases viscosity and promotes particle sedimentation during storage. This sedimentation phenomenon can cause non-uniform shrinkage during pyrolysis, compromising

dimensional accuracy. Consequently, careful optimization of suspension formulation is essential for achieving the necessary compromise between ceramic content and processing stability for successful stereolithographic fabrication.

The DLP-based 3D printing process has been extensively used to produce ceramic parts. It has been utilized for the fabrication of high-density (97–99 %) complex ceramic parts of zirconia and alumina having Vickers hardness of 13.1 and 17.5 GPa, respectively.[48,49] VPP 3D-printed ceramics have been extensively investigated for biomedical applications.[50-52] A team at Vienna University has developed a commercial DLP-based system, which was named lithography-based ceramic manufacturing (LCM), used for the 3D printing of advanced high-performance ceramics.[53] They have fabricated complex ceramic structures of very fine features ($25 \times 25 \times 25\ \mu m^3$) of alumina and bioglass with relative densities above 90% and good mechanical strength. Other ceramic components of zirconia and β-tricalcium phosphate have also been successfully fabricated with solid loadings of up to 50 vol.%.[54] Cellular ceramic structures of fine feature sizes have been fabricated for applications such as honeycomb catalyst supports,[54] heat exchangers,[55] and metamaterial structures with negative Poisson's ratio.[56] Chen's group at Shenzhen University has also manufactured various porous structural components using DLP-based 3D printing and a number of ceramic slurries, including SiC/SiOC composites, Li_4SiO_4, cordierite, and luminescent ceramics,[57-59] particularly for the fabrication of lattice structures with improved performance, as shown in Figure 6.

Light scattering by ceramic particles presents a fundamental challenge in SL, causing lateral curing resolution degradation and altered interlayer bonding characteristics.[60] The achievable curing depth depends on multiple factors including particle size distribution, solid loading percentage, irradiation intensity, and refractive index properties.[54] Crucially, minimizing the refractive index difference between the ceramic filler and resin matrix is vital for achieving high-resolution features, as significant mismatches can compromise printability.[61,62]

This technology has enabled the production of both dense and porous ceramic components with complex architectures for diverse applications ranging from foundry molds to electronic devices and biomedical implants.[63-66] Recent advancements have focused on three key areas: suspension formulation refinement, printing precision enhancement, and optimized thermal processing protocols.[67-70]

Recently, pre-ceramic polymers instead of ceramic suspensions have received great attention due to their direct

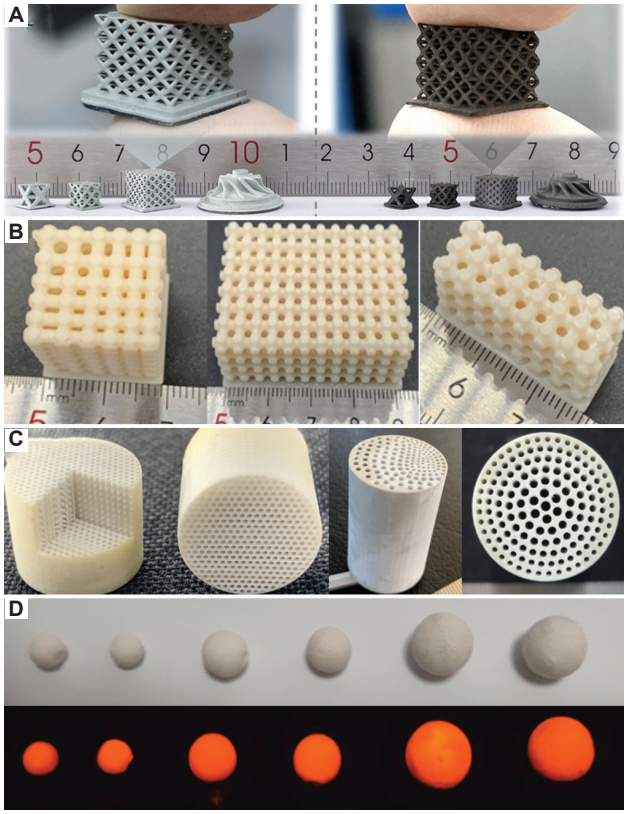

Figure 6. Various components prepared via digital light processing using different ceramic slurries: (A) SiC/SiOC composite lattice structures before and after sintering; (B) Li_4SiO_4 lattice structures; (C) cordierite honeycomb complex structures; (D) luminescent ceramics.

patterning and conversion to ceramic via pyrolysis.[24,71] These advanced ceramics, synthesized through polymer precursor conversion, exhibit superior performance characteristics with tunable functional properties that can be precisely engineered by modifying the pre-ceramic polymer formulation.[72-77] Pre-ceramic polymers offer superior compatibility with printing inks, effectively addressing common challenges related to material non-uniformity and optical interference that typically occur in ceramic particle suspensions. This enhanced formulation enables the fabrication of ceramic components with exceptional surface finish, fine feature resolution, and significant dimensional ratios. Eckel *et al.*[71] developed a UV-curable pre-ceramic polymer system through the combination of mercaptopropyl-methylsiloxane and vinylmethoxysiloxane, incorporating three key additives: a free-radical photoinitiator, radical inhibitor, and UV-absorbing component. The research team successfully employed this resin formulation to produce intricate SiOC ceramic architectures through linear laser SL, followed by pyrolysis at 1000°C under argon protection. Their findings demonstrate that UV-reactive pre-ceramic monomers

suitable for SL can be synthesized by functionalizing organosilicon compounds (siloxanes, silazanes, or carbosilanes) with photopolymerizable groups including thiol, vinyl, acrylate, or methacrylate functionalities.[71] The resin formulation incorporates polymerization inhibitors and UV-absorbing components to precisely control curing depth and reduce light scattering, thereby enhancing feature resolution. This monomer system can be further optimized through the strategic incorporation of metal alkoxides in controlled ratios, enabling the fabrication of advanced composite ceramics. Researchers have successfully extended this methodology to various pre-ceramic polymers, developing efficient production routes for SiCN, silicon nitride, and silicon carbide ceramics that combine dimensional accuracy with cost-effective manufacturing.[61,78-80]

The DLP technique has also been used for printing polymer-derived ceramic (PDC) structures with high resolution and higher efficiency.[81] They prepared dense silicon oxycarbide 3D structures with no cracks and high ceramic yield and micrometer resolution using engineered photosensitive methyl-silsesquioxane pre-ceramic polymer. The printed structures were converted into ceramics in a controlled pyrolysis process, which involves heating to 1000°C for 60 min under nitrogen gas protection with a precisely maintained temperature ramp of 1°C/min.

SiBCN ceramic components have been fabricated with tuned polyborosilazane.[82] A ceramic yield of 58% was obtained after pyrolysis at 1500°C while retaining the shape. The measured weight loss was found to be only 0.35% after pyrolysis, and the highest hardness of 7.8 ± 0.3 GPa with a bulk density of 1.84 ± 0.01 g/cm^3 was achieved. Furthermore, various printable pre-ceramic precursors have been prepared by adding functional groups to the polymer backbones,[80] mixing vinyl/allyl,[61] and physically mixing organosilicones of high ceramic yield with dispersant diluents, monomer, *etc.*[76] An approach different from the free radical polymerization has been proposed by Wang *et al.*,[83] which was introduced with thiol-ene click chemistry-based SL method to produce ceramics upon thermal treatment. The pre-ceramic precursor preparation involves the mixing of polysiloxane and allylhydridopolycarbosilane with phenylbis (2,4,6-trimethylbenzoyl) phosphine oxide (BAPOs) as photoinitiator. Sudan Orange G has been used as a photo-absorber, whereas hydroquinone is a free radical scavenger.[83] After homogenization, the pre-ceramic mixture was functionalized with thiol groups using 1,6-hexanedithiol. The fabricated SiOC ceramic components achieved complete densification without detectable microporosity, demonstrating a remarkable compressive strength of 216 MPa while maintaining a low cellular density of 0.61 g/cm^3. This technique utilizes thiol-ene click chemistry to modify pre-ceramic polymers containing unsaturated bonds (*e.g.*, polysiloxanes, polycarbosilanes, and polycarbosilazanes). During pyrolysis, the printed structures undergo controlled conversion into dimensionally stable thermosets and subsequently into dense glass ceramics with homogeneous shrinkage behavior, maintaining excellent shape retention. The process enables rapid production of pre-ceramic components that yield defect-free, high-density ceramics with superior surface quality after thermal treatment. Brodnik *et al.*[84] demonstrated that pyrolysis behavior varies significantly across different printed geometries, exhibiting structure-dependent shrinkage patterns and mechanical properties – contrasting with earlier assumptions of uniform dimensional changes in pre-ceramic polymer conversion. Fabrication of SiCN ceramic microreactors from polysilazane has been demonstrated by Gyak *et al.*[85] for application in hydrogen generation with ammonia cracking. The researchers developed a novel pre-ceramic processing method involving methacrylate-functionalized polyvinylsilazane combined with a ternary photoinitiator system {2,2-dimethoxy-2-phenylacetophenone, 2-hydroxy-2-methylpropiophenone, diphenyl(2,4,6-trimethylbenzoyl)-phosphine oxide in 3:1:1 ratio} dissolved in toluene. This approach enables the fabrication of advanced functional ceramics with exceptional performance characteristics suitable for extreme operating environments. Researchers have successfully engineered composite ceramic materials by introducing functional additives into pre-ceramic systems. Schmidt *et al.*[86] demonstrated this approach by dispersing alumina particles within a silicone-based pre-ceramic matrix, which upon pyrolysis transformed into porous mullite ceramics with unique rhombicuboctahedral morphology. The resulting 3D-printed mullite components exhibited a compressive strength of 1.8 ± 0.3 MPa, achieving a bulk density of 3.1 g/cm^3 while maintaining an exceptionally high porosity level of 90% by volume.

Chen's group from Shenzhen University has carried out research on the preparation of PDC precursor photosensitive resins and their DLP 3D printing (Figure 7). A low-viscosity and high-curing-strength silicone-based photosensitive resin co-doped with Zr/Ti was synthesized using the sol-gel method.[77] Compact SiOC lattice structures were obtained by pyrolysis at high temperatures in a nitrogen environment. The evolution of phase composition and microstructure was characterized. Their results showed that the compressive strength of lattice structure ceramics was significantly improved as temperature augmented, and the high concentration of metal doping further improved

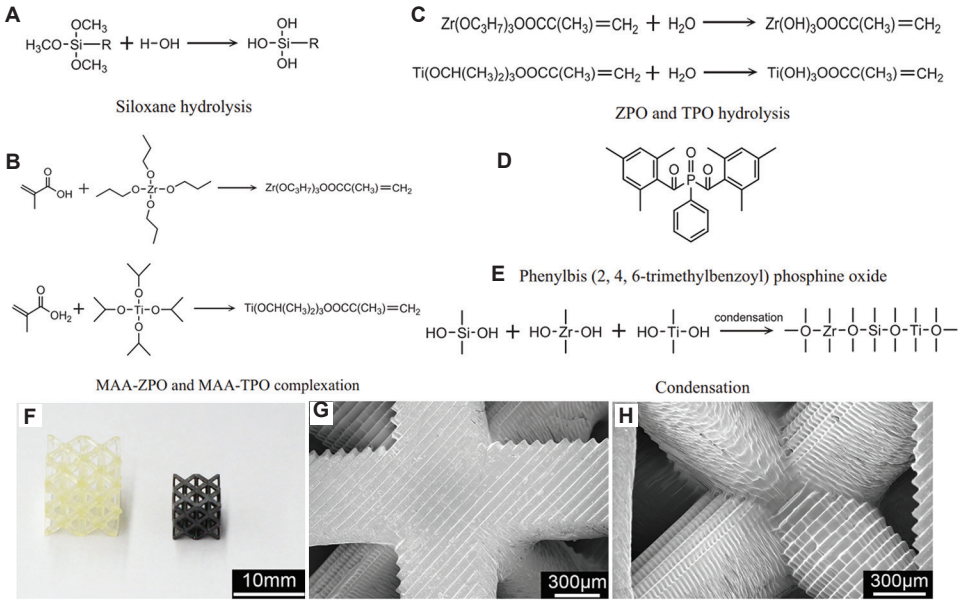

Figure 7. Material synthesis, 3D printed and pyrolyzed SiOC ceramics. The synthesis pathway is illustrated in panel (A-E), showing reagent molecular configurations and the sol-gel transition process that generates the inorganic network. (F) Images displaying the as-printed polymer precursor and its pyrolyzed SiOC ceramic counterpart for comparison purposes. (G and H) Microstructural characterizations revealing surface morphology and fracture patterns of the pyrolyzed octet-truss SiOC ceramic architecture processed at 1000°C.[77] Copyright © 2018 Elsevier. Reprinted with permission of Elsevier

the compressive strength. In addition, zirconium-based photosensitive resin was synthesized with metal alkyls, and a new zirconium-based photosensitive resin suitable for DLP 3D printing was obtained by optimizing the ratio of each component of the resin, and a porous lattice structure ZrOC ceramic with high specific strength was successfully prepared. By comparing the macroscopic photos of the samples treated at different pyrolysis temperatures, it can be found that the product shrank evenly after pyrolysis, showing a smooth surface and no clogging and cracks inside. The shrinkage rate increased continuously with the rise of pyrolysis temperature, concomitant with continuous improvement of the product's mechanical properties. Thus, various metallic precursors such as Fe, Ni, Co, and Pt can be incorporated into pre-ceramics to obtain PDCs for specific applications.

To address the complexity of existing photopolymerizable ceramic precursor material formulations and processes, Chen's group proposed a simplified approach using three commercially available low-cost organic polysiloxane ceramic precursors containing different functional groups/substituents as silicon sources.[76] Through a straightforward physical blending process, they developed photosensitive resin formulations for ceramic precursors. The research focused on investigating key properties and mechanisms including rheological behavior, stability, printability, and pyrolysis-induced ceramic quality of these precursor resins. By optimizing the printing process and sintering parameters to achieve both lightweight strength and structural precision requirements, the group successfully designed and fabricated various lattices. After pyrolysis, fully dense SiOC ceramics with high structural integrity, fine surface finish, and exceptionally high carbon-to-oxygen ratios were formed. Notably, the octagonal lattice-structured SiOC ceramics demonstrated a remarkable apparent density of 0.33 g/cm^3 and a specific strength reaching 5.74 × 10^4 N·m/kg, significantly outperforming previously reported material systems with comparable densities (Figure 8). This study provides robust theoretical and technical support for achieving lightweight yet high-strength complex ceramic precursor components. The breakthrough lies in establishing a material-process-performance framework that enables precise control over structural lightweight and mechanical enhancement in polymer-derived ceramics, opening new possibilities for advanced ceramic applications requiring intricate geometries and superior mechanical properties.

More recently, the research group also developed a novel two-stage folding-assisted pyrolysis strategy for 4D printing of shape-programmable PDCs.[88] A two-step thermal process (300°C pre-pyrolysis followed by 1000°C ceramization) enables controlled deformation and crack mitigation. The first stage fixes folded shapes via partial decomposition of organic components while creating microchannels for gas release, eliminating stress from metal wire fixatives. The second stage achieves

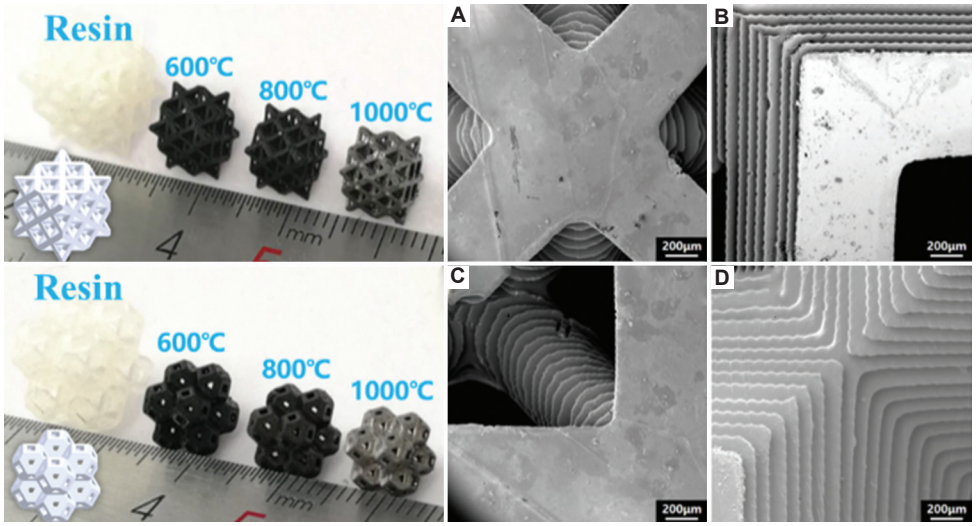

Figure 8. Lattice structures after printing and pyrolysis at different temperatures. Left: digital models and sample photos. Right: (A-D) Microscopic images of the detailed surface features after pyrolysis[76] (diagrams reused under the terms of the Creative Commons CC-BY license) During the pyrolysis of polymer-derived ceramics, the decomposition of organic functional groups generates small molecular gases that continuously and disorderly escape from the structure. This uncontrolled gas release often leads to defects such as cracking, warping, and structural collapse, severely limiting dimensional accuracy, surface morphology, and achievable component size – a critical challenge in precursor-derived ceramic additive manufacturing. To address this issue, Chen's group[87] proposed an innovative approach by introducing low-melting-point additives or specific organic modifiers into the photosensitive resin formulation. These additives create physical microchannels during pyrolysis through their own continuous gas emission, providing organized pathways for the controlled release of macromolecular decomposition gases. This mechanism effectively mitigates internal stress accumulation, thereby suppressing crack formation, minimizing dimensional distortion, and preventing structural collapse. Consequently, precursor-derived ceramic components with enhanced precision, improved surface roughness, reduced warpage, and increased critical thickness (cellular skeleton thickness exceeding 2 mm and bulk body thickness surpassing 5 mm) have been successfully fabricated, as demonstrated in Figure 9. Compared with conventional crack-control techniques such as hot pressing, hot isostatic pressing, and spark plasma sintering, this method offers distinct advantages including simplified processing (ambient pressure operation), reduced cycle time, and cost-effectiveness.

full ceramization into dense SiOC. Despite a low ceramic yield rate (13.5 wt.%) and significant shrinkage (59.91%), the method successfully produces crack-free, geometrically complex ceramics through UV-curable resin design and stress management. Flexible green bodies from photopolymerization allow manual folding into intricate shapes (*e.g.*, spirals, flowers) that retain structural integrity after pyrolysis (Figure 10). Material characterization confirms chemical bond evolution, microchannel formation, and defect-free microstructures, while mechanical testing reveals a compressive strength of 21.31 MPa. This strategy bridges additive manufacturing and ceramic processing, enabling high-precision, defect-resistant PDCs for aerospace and biomedical applications.

TPP has also been explored at a large scale for the fabrication of polymeric materials for optical applications; however, the requirement of complex micro/nanostructures for application in harsh environments has led to the exploration of TPP for the fabrication of advanced ceramic components. Pre-ceramic polymers have been proven to be a suitable candidate for fabricating complex structures using TPP and their direct conversion to ceramic counterparts via pyrolysis. The limitation is the shrinkage of pre-ceramic polymers during pyrolysis and hence various parameters, such as temperature, heating rate, and composition, must be controlled. 3D SiCN nano/microstructures in a resolution of a few hundreds of nanometers were first fabricated by Pham *et al.*[89] using TPP an inorganic pre-ceramic polymer with a linear shrinkage of ~ 41%. Further, they resolved the issue of shrinkage by incorporating 10 nm silica particles into the pre-ceramic polymer and were able to achieve nearly zero shrinkage of the final ceramic component for a solid content of 40 wt.%.

The TPP technique has been employed as a template-based approach for producing hollow ceramic nanolattices. This technique involves three key steps: (i) TPP fabrication of nanoscale polymer molds, (ii) conformal deposition of ceramic materials (TiN, Al_2O_3) via vapor-phase techniques, and (iii) precision opening of the structure using ion-beam milling followed by template removal through chemical or plasma etching.[90] Thus, TPP in conjunction with appropriate photosensitive pre-ceramic polymers enables fabrication of complex 3D structures of extremely high-accuracy sub-wavelength features, which are otherwise not possible with other SL techniques. The challenge associated with this is the difficulty in detaching components from the

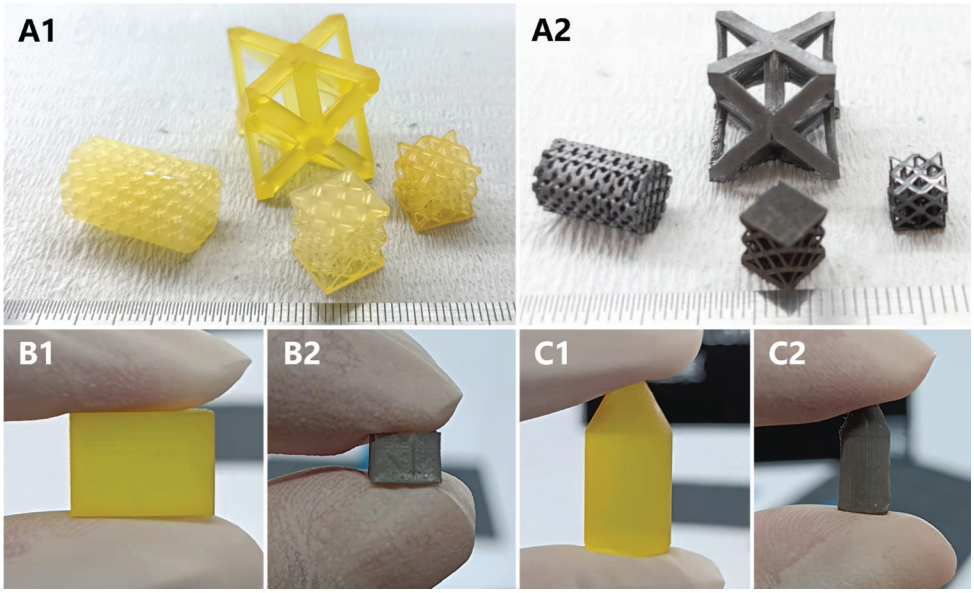

Figure 9. Samples before and after pyrolysis: (A1 and A2) cellular components, (B1 and B2) block, (C1 and C2) bullet

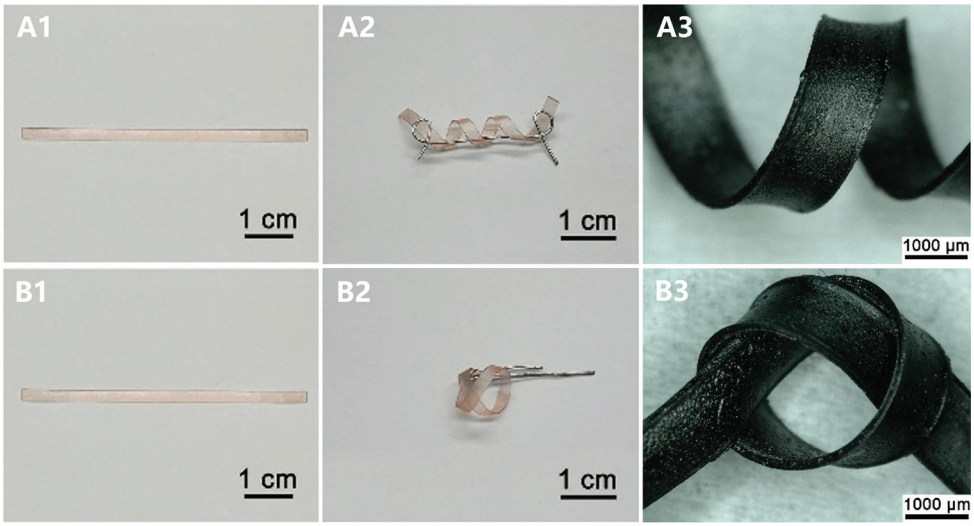

Figure 10. Programmable shapes of printed samples after printing, folding, and folding-assisted two-stage pyrolysis: (A1-A3) shapes of spirals, (B1-B3) shapes of knots

build platform to obtain free-standing components, thereby limiting the pyrolysis temperature to 600°C. The TPP is only applicable to slurries transparent to infrared light and the fabrication of opaque slurries is challenging. In addition, the problem of shrinkage during pyrolysis can be resolved by the incorporation of nanofillers or using a low-shrinkage pre-ceramic polymer.[89] The printed components using TPP are of small sizes and generally require longer production owing to the slow fabrication speed.

The CLIP technique leverages an oxygen-inhibited polymerization zone to enable rapid curing of photopolymer resins. The technology's primary constraints involve resin curing kinetics and flow dynamics within the build area – parameters requiring optimization to fully realize CLIP's revolutionary potential for cost-effective manufacturing of intricate polymer components through additive processes.

These studies showed that the VPP techniques are compatible with producing ceramic parts from pre-ceramic and various ceramic powders together with resins. Micro- to nano-architected ceramic materials of complex shapes can be produced with excellent specific stiffness and strength, which may find application in many areas of science and technology.

Table 3. Application fields for vat photopolymerization 3D-printed ceramics

Application fields	Examples
Biomedicines	Artificial bones, implants, teeth, dental crowns, veneers, orthodontic brackets, etc.
Aerospace	Turbine blades, radomes, combustors, heat insulation tiles, electromagnetic wave shielding components, etc.
Energy	Solid oxide fuel cells, lithium-ion batteries, nuclear fusion tritium breeders, supercapacitors, etc.
Electronics	Smart watch frames, smartphone back panels, delicate components for electronic devices
Cultural products	Jewelry, antique restoration and preservation, customized prototypes and gadgets

6. Conclusion and perspectives

The VPP techniques have emerged as a powerful tool for the additive manufacturing of ceramics, offering unprecedented capabilities in producing complex structures with high precision and resolution. The integration of pre-ceramic polymers and ceramic slurries has significantly expanded the scope of applications, enabling the fabrication of advanced ceramic components with properties tailored for various industries, including biomedical, electronics, aerospace, and energy (Table 3). These techniques have demonstrated the potential to overcome traditional manufacturing limitations, providing a cost-effective and efficient approach to producing high-performance ceramics without the need for additional tooling. The advantages of VPP are multifaceted. The high resolution and fast printing speed make it suitable for creating intricate geometries and microstructures, which are challenging to achieve with conventional manufacturing methods. The ability to produce complex shapes with minimal waste and short production cycles further enhances its appeal. Moreover, the use of pre-ceramic polymers has opened up new possibilities for creating ceramics with exceptional mechanical and thermal properties, as well as multifunctional composites that can be tailored for specific applications. However, despite the significant progress made, several challenges remain. The absorption and scattering of light by ceramic particles can significantly affect the printing quality, leading to issues such as reduced curing depth and increased curing width. This can result in decreased dimensional accuracy and resolution, requiring careful optimization of printing parameters to mitigate these effects. In addition, the ceramic powder dispersion in the slurry, the viscosity, and the stability of the slurry over time are critical factors that need to be addressed to ensure consistent and high-quality prints.

Future work should focus on optimizing the composition and rheology of ceramic slurries and pre-ceramic polymers to enhance printability and reduce defects. The development of new photoinitiators and additives that can improve the photoreactivity of the materials while minimizing light scattering is crucial. Advanced testing techniques, such as *in situ* monitoring and computational modeling, can offer stronger insights into the curing mechanisms and help in the optimization of printing parameters. This will enable more precise control over the manufacturing process, enabling the production of ceramic components with higher quality and stability. Furthermore, the exploration of new applications and materials is essential for the continued growth of VPP in the ceramics field. The fabrication of microreactors, metamaterials, and bioactive scaffolds represents promising areas for future research, with the potential to revolutionize various industries. The development of new ceramic materials with enhanced properties, such as higher strength, improved thermal stability, and advanced functional characteristics, will further expand the scope of applications. In addition, the environmental and economic aspects of VPP should be considered. The use of non-toxic and environmentally friendly materials, as well as the development of more efficient and sustainable manufacturing processes, will be important for the long-term success of this technology. The reduction of waste and energy consumption, along with the optimization of production costs, will make VPP a more viable and attractive option for industrial applications.

As the technology continues to evolve, it is expected to play a pivotal role in the additive manufacturing of high-performance ceramics, contributing to advancements in various scientific and technological fields. The ongoing efforts in this area are likely to induce breakthroughs that will further enhance the capabilities and applications of VPP, making it a valuable tool in the manufacturing of advanced ceramics.

Acknowledgments

None.

Funding

This work was financially supported by the Key Project of the Department of Education of Guangdong Province (2022ZDZX3017), the Special Support Plan of Guangdong Province (2021TQ05Z151), Guangdong Basic and Applied Basic Research Foundation (2024A1515010049), and SZU Research Fund (GFPY-YB-2024-03).

Conflicts of interest

Zhangwei Chen serves as the Editorial Board Member of the journal but was not in any way involved in the

editorial and peer-review process conducted for this paper, directly or indirectly. Other authors declare they have no competing interests.

Author's contributions

Investigation: Chongyu Long
Data curation: Chongyu Long
Formal analysis: Chongyu Long
Funding acquisition: Zhangwei Chen
Investigation: Zhiyuan Liu, Changyong Liu, Zhangwei Chen
Resources: Zhangwei Chen
Supervision: Zhangwei Chen
Visualization: Chongyu Long
Writing–original draft: Chongyu Long, Zhangwei Chen
Writing–review & editing: All authors

Ethics approval and consent to participate

Not applicable.

Consent for publication

Not applicable.

Availability of data

Not applicable.

References

1. Lee JY, An J, Chua CK. Fundamentals and applications of 3D printing for novel materials. *Appl Mater Today*. 2017;7:120-133.

   doi: 10.1016/j.apmt.2017.02.004

2. Chen Z, Li Z, Li J, *et al.* 3D printing of ceramics: A review. *J Eur Ceram Soc*. 2019;39(4):661-687.

   doi: 10.1016/j.jeurceramsoc.2018.11.013

3. Davoudinejad A. Vat photopolymerization methods in additive manufacturing. In: *Additive Manufacturing*. Netherlands: Elsevier; 2021. p. 159-181.

   doi: 10.1016/B978-0-12-818411-0.00007-0

4. Rahaman MN. *Ceramic Processing and Sintering*. United States: CRC Press; 2017.

   doi: 10.1201/9781315274126

5. Hull CW. Inventor; *Methods and Apparatus for Production of Three-dimensional Objects by Stereolithography. USA Patent US5236637*; 1986.

6. Jacobs PF. *Rapid Prototyping & Manufacturing: Fundamentals of Stereolithography*. United States: Society of Manufacturing Engineers; 1992.

7. Parra-Cabrera C, Achille C, Kuhn S, Ameloot R. 3D printing in chemical engineering and catalytic technology: Structured catalysts, mixers and reactors. *Chem Soc Rev*. 2018;47(1):209-230.

   doi: 10.1039/C7CS00631D

8. Choi JW, Kim HC, Wicker R. Multi-material stereolithography. *J Mater Process Technol*. 2011;211(3):318-328.

   doi: 10.1016/j.jmatprotec.2010.10.003

9. Klein J, Stern M, Franchin G, *et al.* Additive manufacturing of optically transparent glass. *3D Print Addit Manuf*. 2015;2(3):92-105.

   doi: 10.1089/3dp.2015.0021

10. Halloran JW. Ceramic stereolithography: Additive manufacturing for ceramics by photopolymerization. *Annu Rev Mater Res*. 2016;46(1):19-40.

    doi: 10.1146/annurev-matsci-070115-031841

11. Griffith ML, Halloran JW. Ultraviolet curable ceramic suspensions for stereolithography of ceramics. In: *Proceedings Solid Freeform Fabrication Symposium;* 1994. p. 529-534.

12. Nakamoto T, Yamaguchi K. *Consideration on the Producing of High Aspect Ratio Micro Parts using UV Sensitive Photopolymer*. United States: IEEE; 1996. p. 53-58.

13. Bertsch A, Zissi S, Jezequel J, Corbel S, Andre J. Microstereophotolithography using a liquid crystal display as dynamic mask-generator. *Microsyst Technol*. 1997;3(2):42-47.

14. Göppert-Mayer M. Elementary processes with two quantum transitions. *Ann Phys*. 2009;521(7-8):466-479.

    doi: 10.1002/andp.200952107-804

15. Kaiser W, Garrett CGB. Two-photon excitation in CaF2:Eu2+. *Phys Rev Lett*. 1961;7(6):229-231.

    doi: 10.1103/PhysRevLett.7.229

16. Paz VF, Emons M, Obata K, *et al.* Development of functional sub-100 nm structures with 3D two-photon polymerization technique and optical methods for characterization. *J Laser Appl*. 2012;24(4):042004.

    doi: 10.2351/1.4712151

17. Bhawalkar JD, He GS, Prasad PN. Nonlinear multiphoton processes in organic and polymeric materials. *Rep Prog Phys*. 1996;59(9):1041.

    doi: 10.1088/0034-4885/59/9/001

18. LaFratta CN, Fourkas JT, Baldacchini T, Farrer RA. Multiphoton fabrication. *Angew Chem Int Ed*. 2007;46(33):6238-6258.

    doi: 10.1002/anie.200603995

19. Fried JR. *Polymer Science and Technology*. United Kingdom: Pearson Education; 2014.

20. Serbin J, Egbert A, Ostendorf A, *et al.* Femtosecond laser-

induced two-photon polymerization of inorganic-organic hybrid materials for applications in photonics. *Opt Lett*. 2003;28(5):301-303.

doi: 10.1364/ol.28.000301

21. Zipfel WR, Williams RM, Webb WW. Nonlinear magic: Multiphoton microscopy in the biosciences. *Nat Biotechnol*. 2003;21(11):1369-1377.

doi: 10.1038/nbt899

22. Tumbleston John R, Shirvanyants D, Ermoshkin N, *et al*. Continuous liquid interface production of 3D objects. *Science*. 2015;347(6228):1349-1352.

doi: 10.1126/science.aaa2397

23. González-Méijome JM, Compañ-Moreno V, Riande E. Determination of oxygen permeability in soft contact lenses using a polarographic method: estimation of relevant physiological parameters. *Ind Eng Chem Res*. 2008;47(10):3619-3629.

24. Wang G, Song Y. Enhancing the yield of polycarbosilane synthesis via recycling of liquid by-product at atmospheric pressure. *Ceram Int*. 2018;44(6):6474-6478.

doi: 10.1016/j.ceramint.2018.01.101

25. Colombo P, Mera G, Riedel R, Sorarù GD. Polymer-derived ceramics: 40 years of research and innovation in advanced ceramics. *J Am Ceram Soc*. 2010;93(7):1805-1837.

doi: 10.1111/j.1551-2916.2010.03876.x

26. Martínez-Crespiera S, Ionescu E, Schlosser M, *et al*. Fabrication of silicon oxycarbide-based microcomponents via photolithographic and soft lithography approaches. *Sens Actuat A Phys*. 2011;169(1):242-249.

doi: 10.1016/j.sna.2011.04.041

27. Kashimura S, Tane Y, Ishifune M, *et al*. Practical method for the synthesis of polysilanes using Mg and Lewis acid system. *Tetrahedron Lett*. 2008;49(2):269-271.

doi: 10.1016/j.tetlet.2007.11.083

28. Jones RG, Holder SJ. High-yield controlled syntheses of polysilanes by the Wurtz-type reductive coupling reaction. *Polym Int*. 2006;55(7):711-718.

doi: 10.1002/pi.1945

29. Krempner C. Polysilane dendrimers. *Polymers*. 2012;4(1):408-447.

doi: 10.3390/polym4010408

30. Chen J, He G, Liao Z, *et al*. Control of structure formation of polycarbosilane synthesized from polydimethylsilane by Kumada rearrangement. *J Appl Polym Sci*. 2008;108(5):3114-3121.

doi: 10.1002/app.27847

31. Cheng X, Xie Z, Song Y, Xiao J, Wang Y. Structure and properties of polycarbosilane synthesized from polydimethylsilane under high pressure. *J Appl Polym Sci*. 2006;99(3):1188-1194.

doi: 10.1002/app.22465

32. Lodhe M, Babu N, Selvam A, Balasubramanian M. Synthesis and characterization of high ceramic yield polycarbosilane precursor for SiC. *J Adv Ceram*. 2015;4:307-311.

doi: 10.1007/s40145-015-0169-8

33. He L, Zhang Z, Yang X, Jiao L, Li Y, Xu C. Liquid polycarbosilanes: synthesis and evaluation as precursors for SiC ceramic. *Polym Int*. 2015;64(8):979-985.

doi: 10.1002/pi.4904

34. Hörz M, Zern A, Berger F, *et al*. Novel polysilazanes as precursors for silicon nitride/silicon carbide composites without "free" carbon. *J Eur Ceram Soc*. 2005;25(2-3):99-110.

doi: 10.1016/j.jeurceramsoc.2004.05.003

35. Blum YD, Schwartz KB, Laine RM. Preceramic polymer pyrolysis: Part 1 Pyrolytic properties of polysilazanes. *J Mater Sci*. 1989;24:1707-1718.

doi: 10.1007/BF01138991

36. Kroke E, Li YL, Konetschny C, Lecomte E, Fasel C, Riedel R. Silazane derived ceramics and related materials. *Mater Sci Eng R Rep.* 2000;26(4-6):97-199.

doi: 10.1016/S0927-796X(00)00013-0

37. Soraru GD. Silicon oxycarbide glasses from gels: Code: H1. *J Sol Gel Sci Technol*. 1994;2:843-848.

doi: 10.1007/BF00489675

38. Schmitt M. Analysis of silanes and of siloxanes formation by Raman spectroscopy. *RSC Adv*. 2014;4(4):1907-1917.

doi: 10.1039/C3RA45816A

39. Mera G, Riedel R, Poli F, Müller K. Carbon-rich SiCN ceramics derived from phenyl-containing poly (silylcarbodiimides). *J Eur Ceram Soc*. 2009;29(13):2873-2883.

doi: 10.1016/j.jeurceramsoc.2009.03.020

40. Widgeon S, Mera G, Gao Y, *et al*. Nanostructure and energetics of carbon-rich SiCN ceramics derived from polysilylcarbodiimides: Role of the nanodomain interfaces. *Chem Mater*. 2012;24(6):1181-1191.

doi: 10.1021/cm3000259

41. Gao Y, Mera G, Nguyen H, Morita K, Kleebe HJ, Riedel R. Processing route dramatically influencing the nanostructure of carbon-rich SiCN and SiBCN polymer-derived ceramics. Part I: Low temperature thermal transformation. *J Eur Ceram Soc*. 2012;32(9):1857-1866.

doi: 10.1016/j.jeurceramsoc.2012.01.022

42. Zhang Z, Zeng F, Han J, Luo Y, Xu C. Synthesis and characterization of a new liquid polymer precursor for Si-B-C-N ceramics. *J Mater Sci*. 2011;46:5940-5947.

doi: 10.1007/s10853-010-4934-1

43. Widgeon S, Mera G, Gao Y, Sen S, Navrotsky A, Riedel R. Effect of precursor on speciation and nanostructure of SiBCN polymer-derived ceramics. *J Am Ceram Soc*. 2013;96(5):1651-1659.

doi: 10.1111/jace.12217

44. Griffith ML, Halloran JW. Freeform fabrication of ceramics via stereolithography. *J Am Ceram Soc*. 1996;79(10):2601-2608.

doi: 10.1111/j.1151-2916.1996.tb09022.x

45. Schwartz KB, Rowcliffe DJ. Modeling density contributions in preceramic polymer/ceramic powder systems. *J Am Ceram Soc*. 1986;69(5):C-106.

doi: 10.1111/j.1151-2916.1986.tb04782.x

46. Wang WL, Cheah CM, Fuh JYH, Lu L. Influence of process parameters on stereolithography part shrinkage. *Mater Design*. 1996;17(4):205-213.

doi: 10.1016/S0261-3069(97)00020-1

47. Travitzky N, Bonet A, Dermeik B, *et al*. Additive manufacturing of ceramic-based materials. *Adv Eng Mater*. 2014;16(6):729-754.

doi: 10.1002/adem.201400097

48. He R, Liu W, Wu Z, *et al*. Fabrication of complex-shaped zirconia ceramic parts via a DLP- stereolithography-based 3D printing method. *Ceram Int*. 2018;44(3):3412-3416.

doi: 10.1016/j.ceramint.2017.11.135

49. Zhou M, Liu W, Wu H, *et al*. Preparation of a defect-free alumina cutting tool via additive manufacturing based on stereolithography - Optimization of the drying and debinding processes. *Ceram Int*. 2016;42(10):11598-11602.

doi: 10.1016/j.ceramint.2016.04.007

50. Li S, Shan Y, Chen J, *et al*. 3D printing and biomedical applications of piezoelectric composites: A critical review. *Adv Mater Technol*. 2025;10(5):2401160.

51. Hamza M, Kanwal Q, Hussain MI, *et al*. Recent progress in 3D printed piezoelectric materials for biomedical applications. *Mater Sci Eng R Rep*. 2025;164:100962.

52. Zhang P, He R. 3D-printed silicon nitride ceramic implants for clinical applications: The state of the art and prospects. *RSC Adv*. 2025;15(1):406-419.

53. Scheithauer U, Schwarzer E, Ganzer G, *et al*. Microhreactors made by lithography-based ceramic manufacturing (LCM). In: *Additive Manufacturing and Strategic Technologies in Advanced Ceramics: Ceramic Transactions*. Vol. 258. United States: Wiley; 2015. p. 31-41.

doi: 10.1002/9781119183860.ch3

54. Schwentenwein M, Homa J. Additive manufacturing of dense alumina ceramics. *Int J Appl Ceram Technol*. 2015;12(1):1-7.

doi: 10.1111/ijac.12324

55. Scheithauer U, Schwarzer E, Moritz T, Michaelis A. Additive manufacturing of ceramic heat exchanger: Opportunities and limits of the lithography-based ceramic manufacturing (LCM). *J Mater Eng Perform*. 2018;27(1):14-20.

doi: 10.1007/s11665-017-3056-1

56. Lantada AD, de Blas Romero A, Schwentenwein M, Jellinek C, Homa J. Lithography-based ceramic manufacture (LCM) of auxetic structures: Present capabilities and challenges. *Smart Mater Struct*. 2016;25(5):054015.

doi: 10.1088/0964-1726/25/5/054015

57. Qu P, Liang G, Hussain MI, *et al*. Low-temperature fabrication of high-specific strength SiC-based ceramics via photopolymerization 3D printing with controllable anisotropy. *Int J Extreme Manuf*. 2025;7(5):055002.

doi: 10.1088/2631-7990/add2e1

58. Luo X, Ren W, Xing H, Hussain MI, Chen Z. Additively manufactured Li4SiO4 ceramic pebbles with radial pores for enhanced performance. *Ceram Int*. 2025.

doi. 10.1016/j.ceramint.2025.01.332

59. Ren W, Liu W, Luo X, Liu Z, Liu C, Chen Z. 3D printing of cordierite glass-ceramics. *Ceram Int*. 2025;51(2):1632-1642.

60. Gentry SP, Halloran JW. Depth and width of cured lines in photopolymerizable ceramic suspensions. *J Eur Ceram Soc*. 2013;33(10):1981-1988.

doi: 10.1016/j.jeurceramsoc.2013.02.012

61. de Hazan Y, Penner D. SiC and SiOC ceramic articles produced by stereolithography of acrylate modified polycarbosilane systems. *J Eur Ceram Soc*. 2017;37(16):5205-5212.

doi: 10.1016/j.jeurceramsoc.2017.03.021

62. Badev A, Abouliatim Y, Chartier T, *et al*. Photopolymerization kinetics of a polyether acrylate in the presence of ceramic fillers used in stereolithography. *J Photochem Photobiol A*. 2011;222(1):117-122.

doi: 10.1016/j.jphotochem.2011.05.010

63. Leigh SJ, Purssell C, Bowen J, Hutchins DA, Covington JA, Billson D. A miniature flow sensor fabricated by micro-stereolithography employing a magnetite/acrylic nanocomposite resin. *Sens Actuat A*. 2011;168(1):66-71.

doi: 10.1016/j.sna.2010.12.007

64. Chen W, Kirihara S, Miyamoto Y. Fabrication and measurement of micro three-dimensional photonic crystals of SiO2 ceramic for terahertz wave applications. *J Am Ceram Soc*. 2007;90(7):2078-2081.

doi: 10.1111/j.1551-2916.2007.01724.x

65. Du D, Asaoka T, Ushida T, Furukawa KS. Fabrication and perfusion culture of anatomically shaped artificial bone using stereolithography. *Biofabrication*. 2014;6(4):045002.

doi: 10.1088/1758-5082/6/4/045002

66. Lian Q, Sui W, Wu X, Yang F, Yang S. Additive manufacturing of ZrO2 ceramic dental bridges by stereolithography. *Rapid Prototyp J*. 2018;24(1):114-119.

doi: 10.1108/RPJ-09-2016-0144

67. Bae CJ, Halloran JW. Influence of residual monomer on cracking in ceramics fabricated by stereolithography. *Int J Appl Ceram Technol*. 2011;8(6):1289-1295.

doi: 10.1111/j.1744-7402.2011.02611.x

68. Bae CJ, Ramachandran A, Halloran JW. Quantifying particle segregation in sequential layers fabricated by additive manufacturing. *J Eur Ceram Soc*. 2018;38:4082-4088.

doi: 10.1016/j.jeurceramsoc.2018.07.040

69. Mitteramskogler G, Gmeiner R, Felzmann R, *et al*. Light curing strategies for lithography-based additive manufacturing of customized ceramics. *Addit Manuf*. 2014;1:110-118.

doi: 10.1016/j.addma.2014.08.004

70. Pfaffinger M, Mitteramskogler G, Gmeiner R, Stampfl J. *Thermal Debinding of Ceramic-filled Photopolymers*. Switzerland: Trans Tech Publ; 2015. p. 75-81.

doi: 10.1002/9781119183860.ch10

71. Eckel ZC, Zhou C, Martin JH, Jacobsen AJ, Carter WB, Schaedler TA. Additive manufacturing of polymer-derived ceramics. *Science*. 2016;351(6268):58-62.

doi: 10.1126/science.aad2688

72. Chaudhary RP, Parameswaran C, Idrees M, *et al*. Additive manufacturing of polymer-derived ceramics: Materials, technologies, properties and potential applications. *Prog Mater Sci*. 2022;128:100969.

doi: 10.1016/j.pmatsci.2022.100969

73. Toma L, Kleebe HJ, Müller MM, *et al*. Correlation between intrinsic microstructure and piezoresistivity in a SiOC polymer-derived ceramic. *J Am Ceram Soc*. 2012; 95(3):1056-1061.

doi: 10.1111/j.1551-2916.2011.05026.x

74. Colombo P, Bernardo E, Parcianello G. Multifunctional advanced ceramics from preceramic polymers and nano-sized active fillers. *J Eur Ceram Soc*. 2013;33(3):453-469.

doi: 10.1016/j.jeurceramsoc.2012.10.006

75. Kim KJ, Eom JH, Kim YW, Seo WS. Electrical conductivity of dense, bulk silicon-oxycarbide ceramics. *J Eur Ceram Soc*. 2015;35(5):1355-1360.

doi: 10.1016/j.jeurceramsoc.2014.12.009

76. Li Z, Chen Z, Liu J, *et al*. Additive manufacturing of lightweight and high-strength polymer-derived SiOC ceramics. *Virtual Phys Prototyp*. 2020;15(2):163-177.

doi: 10.1080/17452759.2019.1710919

77. Fu Y, Xu G, Chen Z, Liu C, Wang D, Lao C. Multiple metals doped polymer-derived SiOC ceramics for 3D printing. *Ceram Int*. 2018;44(10):11030-11038.

doi: 10.1016/j.ceramint.2018.03.075

78. Zocca A, Gomes CM, Staude A, Bernardo E, Günster J, Colombo P. SiOC ceramics with ordered porosity by 3D-printing of a preceramic polymer. *J Mater Res*. 2013;28(17):2243-2252.

doi: 10.1557/jmr.2013.129

79. Zhou S, Mei H, Chang P, Lu M, Cheng L. Molecule editable 3D printed polymer-derived ceramics. *Coord Chem Rev*. 2020;422:213486.

doi: 10.1016/j.ccr.2020.213486

80. Hundley JM, Eckel ZC, Schueller E, *et al*. Geometric characterization of additively manufactured polymer derived ceramics. *Addit Manuf*. 2017;18:95-102.

doi: 10.1016/j.addma.2017.09.005

81. Zanchetta E, Cattaldo M, Franchin G, *et al*. Stereolithography of SiOC ceramic microcomponents. *Adv Mater*. 2016;28(2):370-376.

doi: 10.1002/adma.201503470

82. Li S, Duan W, Zhao T, *et al*. The fabrication of SiBCN ceramic components from preceramic polymers by digital light processing (DLP) 3D printing technology. *J Eur Ceram Soc*. 2018;38(14):4597-4603.

doi: 10.1016/j.jeurceramsoc.2018.05.043

83. Wang X, Schmidt F, Hanaor D, Kamm PH, Li S, Gurlo A. Additive manufacturing of ceramics from preceramic polymers: A versatile stereolithographic approach assisted by thiol-ene click chemistry. *Addit Manuf*. 2019;27:80-90.

doi: 10.1016/j.addma.2019.02.012

84. Brodnik NR, Schmidt J, Colombo P, Faber KT. Analysis of multi-scale mechanical properties of ceramic trusses prepared from preceramic polymers. *Addit Manuf*. 2020;31:100957.

doi: 10.1016/j.addma.2019.100957

85. Gyak KW, Vishwakarma NK, Hwang YH, Kim J, Yun HS, Kim DP. 3D-printed monolithic SiCN ceramic microreactors from a photocurable preceramic resin for the high temperature ammonia cracking process. 10.1039/C9RE00201D. *React Chem Eng*. 2019;4(8):1393-1399.

doi: 10.1039/C9RE00201D

86. Schmidt J, Altun AA, Schwentenwein M, Colombo P. Complex mullite structures fabricated via digital light processing of a preceramic polysiloxane with active alumina fillers. *J Eur Ceram Soc*. 2019;39(4):1336-1343.

doi: 10.1016/j.jeurceramsoc.2018.11.038

87. Xiong SF, Liu J, Cao JW, *et al*. 3D printing of crack-free dense polymer-derived ceramic monoliths and lattice skeletons with improved thickness and mechanical performance. *Addit Manuf*. 2022;57:102964.

doi: 10.1016/j.addma.2022.102964

88. Jiang L, Long C, Xiong S, *et al*. 4D printing of shape-programmable polymer-derived ceramics via two-stage folding-assisted pyrolysis strategy. *Virtual Phys Prototyp*. 2024;19(1):e2406408.

doi: 10.1080/17452759.2024.2406408

89. Pham TA, Kim DP, Lim TW, Park SH, Yang DY, Lee KS. Three-dimensional SiCN ceramic microstructures via nano-stereolithography of inorganic polymer photoresists. 2006;16(9):1235-1241.

doi: 10.1002/adfm.200600009

90. Jang D, Meza LR, Greer F, Greer JR. Fabrication and deformation of three-dimensional hollow ceramic nanostructures. *Nat Mater*. 2013;12(10):893.

doi: 10.1038/nmat3738